FULL LENGTH ARTICLE

Eleyon NANOSCALE REPORTS

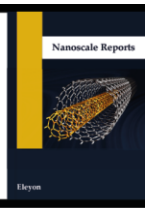

DOI:

Synthesis and Characterization Polyaniline/Cobalt Oxide Nanocomposite by Chemical Oxidation Method

M. Haridevi [a], S. Prabu [a], M. Lakshmi Devi [a], E. Bhakya Lakshmi [a], K. Mohanraj [b], A. Arun [a,*] and M. Kayalvizhi [a,*]

[a] P.G & Research Department of Chemistry, Government Arts College, Tiruvannamalai – 606603, Tamil Nadu, India
[b] Raman Research Laboratory, P.G & Research Department of Physics, Government Arts College, Tiruvannamalai – 606603, Tamil Nadu, India

***Corresponding Author**
kayalpappa78@gmail.com
(M. Kayalvizhi)
Tel.: +91 9486191814

Received : 30-01-2018
Accepted : 12-02-2018

ABSTRACT: The Co_3O_4-PANI nanocomposites has been synthesized by chemical oxidative polymerization method using cobalt chloride. It is a simple and low cost method to prepare nanocomposite. The prepared samples were characterized by using Scanning Electron Microscope (SEM), X-ray diffraction (XRD) and Fourier Transform Spectroscopy (FTIR) to get surface morphology, idea of getting particles of nano sized range so that further characterization can be done, to study the net surface charge of the nanoparticles by Zeta potential, photoluminescence of synthesized nanocomposite and measure photocatalytic activity of the synthesized nanomaterials was successfully tested for photo degradation of dye under UV light were studied.
.

Keywords: Metal oxide nanoparticles; polyaniline; structural properties

1 Introduction

Nanostructures and nanocomposites of conducting polymers have emerged as a new field dedicated to the creation of smart materials for use in future technologies. Today research developments have been focused on modifying conducting polymers structures. The inorganic semiconductors and conducting polymers possess many advantages as low thermal conductivity, high electrical conductivity, cost effectiveness, mass production and extensive area processing. Mutual interactions between inorganic semiconductors and conducting polymers may give rise to interesting properties which are significantly different from those of individual components [1]. Many studies on preparation of polymer nanocomposite have been reported in the quest to develop new advanced materials with improved mechanical, electrical, optical and catalytic properties or to improve conduction mechanism in electronic devices.

Polyaniline (PANI) is a promising conducting polymer due to its easy synthesis, environmental stability and high electrical conductivity on doping with protonic acids [2-3]. The highly ordered structures such as crystalline or self-assembled structures of ideal conducting polymer like electrical conductivity .To induce an ordered structure, other materials acting as filler for the composite are required [4-10]. The preparation of PANI composites with various materials has received great attention because of their unique properties and applications in various electrical and electronic devices. Co_3O_4 is a very important material extensively used in catalysis, gas sensors, electro chromic films, battery cathodes, heterogeneous catalytic materials and magnetic materials [11, 12]. Co_3O_4 nanoparticles have been synthesized by various methods like precipitation method, sol–gel, surfactant-mediated synthesis, thermal decomposition, polymer-matrix assisted synthesis and spray-pyrolysis [13, 14]. Materials based on cobalt oxides have attracted a great interest in view of their technological and fundamental scientific importance [15]. In this paper, we report the preparation and characterization of polymer-cobalt oxide nanocomposites synthesized by in situ oxidative polymerization method.

.

2 Experimental

Aniline was purchased from Merck and was distilled before use for polymerization .All chemicals like potassium persulfate (PPS), Hydrochloric acid, ethanol and acetone were used in experiment were of analytical grade. The chemicals used in the synthesis were $CoCl_2.6H_2O$ and Ammonium hydroxide solution. All the solutions were prepared in double distilled water.

3 Experimental details

3.1. Synthesis of Co_3O_4 Nanoparticles

Co_3O_4 nanoparticles were prepared by chemical precipitation method in which 0.1M $CoCl_2.6H_2O$ (precursor) was added to 100ml of double distilled water with continuous stirring for 2 hour. Then the prepared solution was hydrolyzed by Ammonia drop by drop to maintain the pH =8. The resultant light pink colored precipitates thus obtained were washed with double distilled water and then dried at 100°C in oven for 5 hours. Finally, these were put into the muffle furnace at 600°C for 2 hours. Black color Co_3O_4 nanoparticles were thus obtained

3.2. Synthesis of PANI

Aniline hydrochloride (10mmol) was formed in-situ chemical oxidative method by dissolving aniline in 100ml 1M HCL solution (dopant) stirred vigorously for half an hour at room temperature. The above solution was ice cooled under magnetic stirring condition. Then, catalytic oxidizing agent potassium persulfate having a mole ratio 13mmol dissolved in 50ml of 1M HCl solution was added dropwise to the above solution under stirring condition. The mixture was stirred for 24 h and keeps it as such for complete polymerization. Next day Polyaniline (PANI) precipitate was collected on a filter paper, washed three times with HCL to remove the unreacted aniline and its oligomers from the precipitate. After this process, precipitate was washed three times with 100 ml portions of acetone to absorb the water molecules and for the removal of any residual organic impurities. PANI, synthesized by this method, is formed in its protonated state. The precipitate was firstly dried in air for 30 min and then in oven for 3 hours at 60°C. The product is dried under vacuum and kept in a desiccator.

3.3. Preparation of PANI with Co_3O_4

Aniline hydrochloride (10mmol) was dissolved in 100ml 1M HCL solution (dopant) stirred vigorously for half an hour at room temperature. Then various grams of Co3O4 was added to the reaction mixture and stirred thoroughly. The above solution was ice cooled under magnetic stirring condition. Then, catalytic oxidizing agent potassium persulfate having a mole ratio 13 mmol solution was added drop wise to the above solution under stirring condition. The mixture was stirred for 24 h and keeps it as such for complete polymerization. Next day Polyaniline (PANI) precipitate was collected on a filter paper, washed three times with HCL to remove the unreacted aniline and its oligomers from the precipitate. After this process, precipitate was washed three times with 100 ml portions of acetone to absorb the water molecules and for the removal of any residual organic impurities. PANI/ Co_3O_4, synthesized by this method, are formed in its protonated state. The precipitate was firstly dried in air for 30 min and then in oven for 3 hours at 60°C. The product is dried under vacuum and kept in desiccators. The ratio of polymer/Metal oxide as shown in table.1

Table 1 The ratio of polymer/Metal oxide

Sample Name	Polymer	Oxide	Oxidant
	Aniline (mmol)	Co_3O_4(g)	Potassium Per Sulphate (mmol)
C	-	1	-
P	10	-	13
PC0.01	10	0.01	13
PC0.015	10	0.015	13
PC0.02	10	0.02	13
PC0.025	10	0.025	13

4. Results and discussion

The addition of metal oxides is also important to improve the properties of PANI as they can play different roles than the use of dopants, oxidizing agents and metal ions. Moreover, the use of metal oxides can play significant role to obtain PANI nanofibers not only with good surface

morphological but also with higher and consistence conducting properties.

4.1. X-ray diffraction (XRD) of the Co_3O_4 nanoparticles

Fig.1 shows XRD pattern of the Co_3O_4 nanoparticles. The X-ray diffraction pattern revealed major peaks at 2θ values of 36.43 (311), 21.50 (220), 18.40 (440), corresponding to the simple cubic Co_3O_4 nanoparticles as confirmed by JCPDS card file 073-1701. It is shown in Table 2.Average particle size of the Co_3O_4 nanoparticles was found to be 6.9 nm using Scherrer's formula

Table 2 XRD Data of the Co_3O_4 nanoparticles

S. no	2θ (degree)	FWHM (degree)	β=π/180 * FWHM	2θ= θ/2	D=Kλ/β. Cosθ
1	36.4388	1.21110	0.02112	18.2194	6.9095
2	18.4000	0.00000	0	0	-
3	21.5000	0.00000	0	0	-

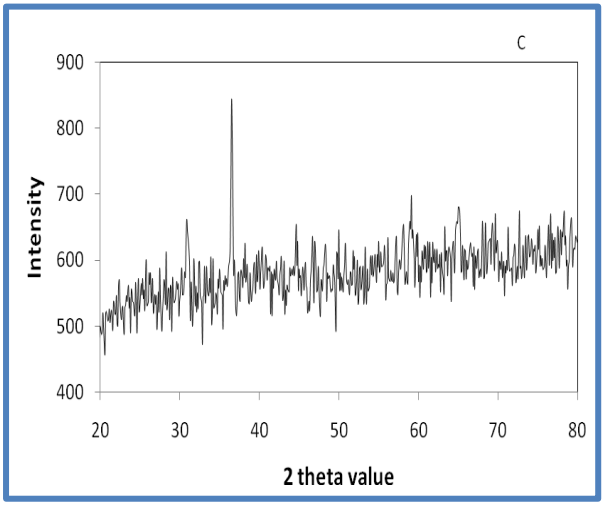

Figure 1 XRD pattern of Co_3O_4 nanoparticles.

4.2 FTIR spectra of the Co3O4 nanoparticles

Fig 2 shows FTIR spectra of Co_3O_4 nanoparticles synthesized by Co-precipitation technique. FTIR spectroscopy was carried out in order to ascertain the purity and nature of metal or metal oxide nanoparticles. FT-IR spectrum of Co_3O_4 nanoparticles showed significant absorption peaks at 525 and 647 cm^{-1}. The absorption band at 525 cm^{-1} was assigned to Co-O stretching vibration mode and 647 cm^{-1} was assigned to the bridging vibration of O-Co-O bond.

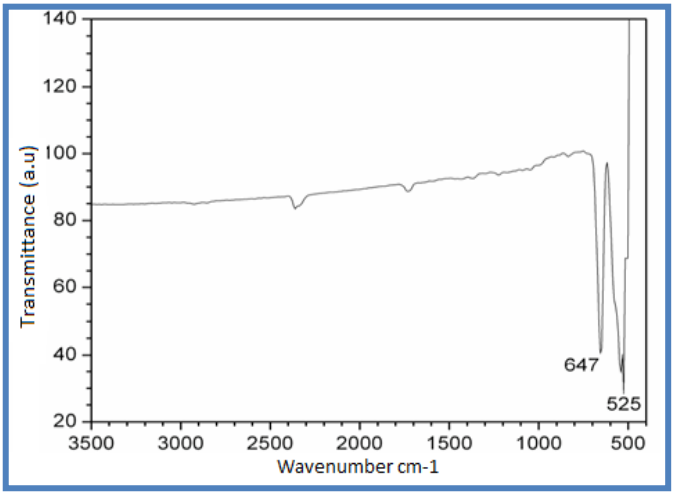

Figure 2. FT IR Spectra of Co3O4 nanoparticles.

4.3. UV-Visible absorption of the Co3O4 nanoparticles

The optical characterization of the sample was recorded on UV-Visible absorption spectrophotometer. Fig 3 shows UV-Visible spectra of Co_3O_4 nanoparticles as a function of wavelength. The UV-Visible absorption spectroscopy of Co_3O_4 nanoparticles shows a absorption peak at about 285 nm corresponding to n-σ* transition of lone pair of electrons of oxygen to Co-O σ- antibonding orbitals.

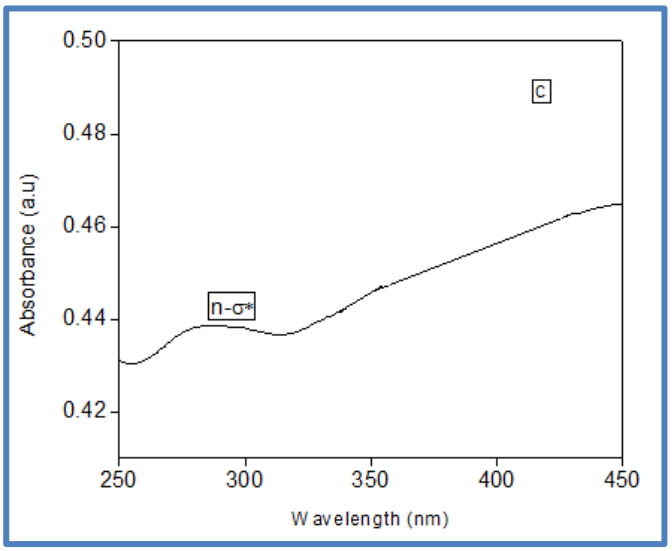

Figure 3 UV Spectra of Co_3O_4 nanoparticles.

4.4. Scanning Electron Microscopy (SEM) of the Co_3O_4 nanoparticles

The morphology and structure of the product were characterized by scanning electron microscopy (SEM). Fig 4 shows a typical SEM image of Co_3O_4 nanoparticles recorded at a different magnification. Among the cluster, there are two needle shaped nanoparticles are shown in fig. In the diameter range of 0.2µm, 1 µm whose resolution range is 55,000 and 20,000, the needle shaped structure is not able to identify whereas the resolution range is decreased to 5000 the needle shaped particles are shown in Figure which its diameter suggests to be about 5micrometers.

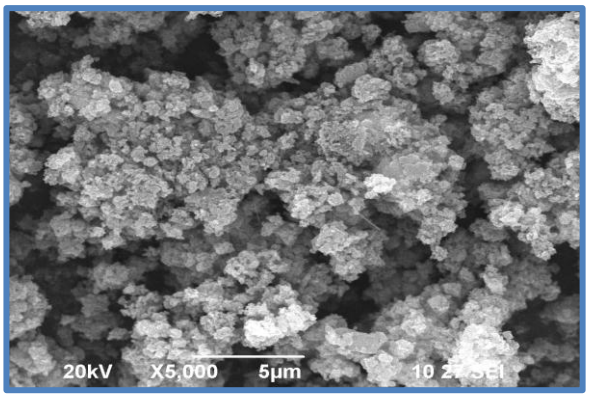

Figure 4. SEM image of Co_3O_4 nanoparticles.

4.5. Photoluminescence of the Co_3O_4 nanoparticles

The photoluminescence spectroscopy (PL) of Co_3O_4 has been performed and spectra are shown in Fig. 5. The PL spectra of Co_3O_4 show peaks in visible region around at 300 nm. In addition, this peak becomes sharp and intense.

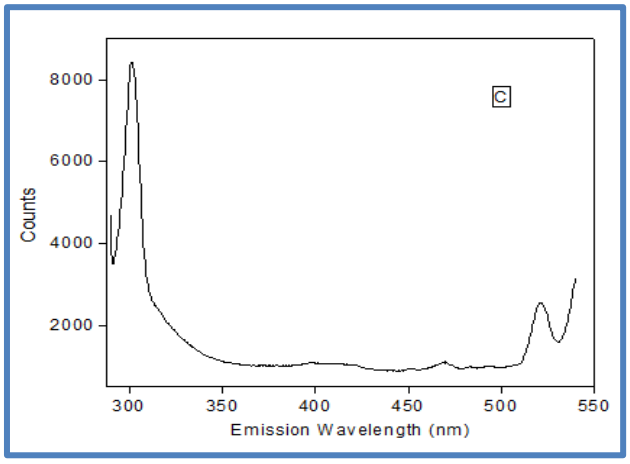

Figure 5 PL images of Co_3O_4 nanoparticles.

5. Undoped PANI and Co_3O_4 doped PANI

5.1 X-Ray Diffraction (XRD) of the undoped and Co_3O_4 doped PANI

XRD spectra of the undoped and Co_3O_4 doped PANI samples P, PC 0.01, PC 0.02 show crystalline quality of all the samples. The XRD pattern of P in figure relieves three strong peaks, observed at 2θ= 26°, 20° and 15° correspond to (110). The peak at 2θ =20° represents the characteristic distance between the ring planes of benzene rings in adjacent chains or the close contact inter-chain distance.

The peak centered at 2θ=26° may be assigned to the scattering from PANI chains at inter planar spacing and very high intensity of the observed peak indicates that the PANI has high crystalline nature .The diffraction peaks of Co_3O_4 nanoparticles and PANI/ Co_3O_4 composites have been indexed to the cubically face center structured Co_3O_4 which were well matched with that in JCPDS, 36-1451. There is no peak for the Co_3O_4 in the composite samples, which indicates that the low percentage of Co_3O_4 does not affect the lattice structure of PANI, similar type of result has been reported in literature [27]. Thus the XRD spectra suggest that during the doping of metal oxides in PANI, it undergoes interfacial interactions with metal crystallites and losses its own morphology. The crystallite size can be estimated with the help of full width at half maximum (FWHM) of the X-ray diffraction data. The broadening of the FWHM is inversely proportional to the average crystallite size, D, as predicted by the wellbeing Scherer's formula. The crystallite size, D, is calculated from the following relation [29]:

$$D = k\lambda/\beta \cos\theta$$

where, λ is the X-ray wavelength; k, the shape factor; D, the average diameter of the crystals in angstroms; θ, the Bragg angle in degree; and β is the line broadening measured by half-height in radian. The value of k depends on several factors including the miller index of the reflection plane and the shape of crystal. If the shape is unknown, k is often considered to be 0.89. The average particle size of P is 2.6nm. The average particle size of PC0.01 and PC0.02 is 3.3 nm and 7.03 nm respectively. This result shows that the metal oxide concentration increases the average particle size also increases. The shifting of the peak's position clearly indicates that Co3O4

nanoparticles are incorporating into the PANI polymer matrix. The X-ray diffraction pattern of the composite revealed that the degree of crystallinity of PANI- Co3O4 composite was higher than that of the PANI as shown in Fig .6.

Table 3 Structural properties of undoped and Co_3O_4 doped PANI

Sample code	2θ (deg)	FWHM (g)	β=π/180* FWHM	2θ= θ/2	D (nm)
P	26.1500	4.50000	0.0785	13.075	1.8133
	20.5000	2.40000	0.0419	10.250	3.3656
	15.2500	2.90000	0.0506	7.625	2.7652
PC0.01	25.6250	2.75000	0.0479	12.812	2.9641
	27.9000	1.80000	0.0314	13.95	4.5500
	14.9000	3.20000	0.0558	7.45	2.5050
PC0.02	25.3300	1.58000	0.0275	12.665	5.1561
	36.0085	0.69410	0.0121	18.454	12.073
	15.1000	1.95000	0.0340	7.55	4.112

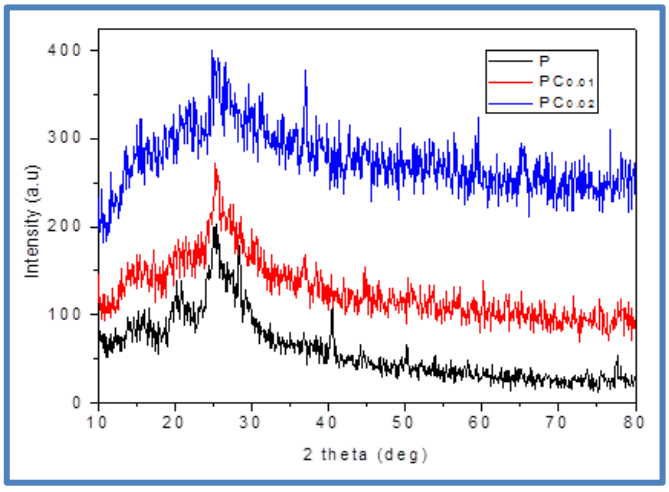

Figure 6 X-ray diffraction (XRD) spectra of the samples P, PC0.01 and PC0.02.

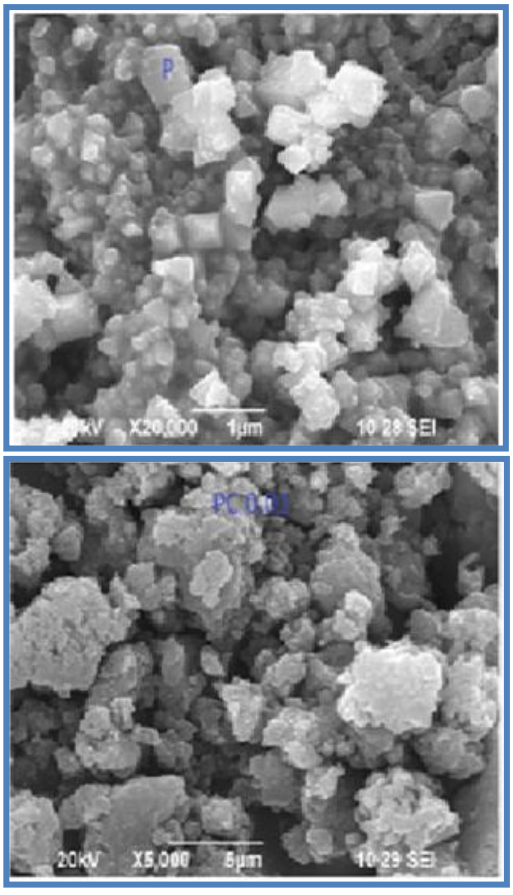

5.2 Scanning Electron Microscopy (SEM) of the undoped and Co_3O_4 doped PANI

Scanning electron microscope (SEM) is used to study the surface morphology of prepared samples. Fig .7 corresponds to P, PC 0.01 to PC 0.02 nanocomposites

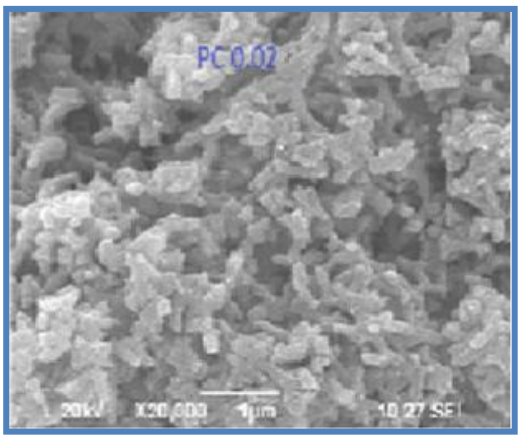

Figure 7. Scanning electron microscope (SEM) images of samples P, PC0.01 and PC 0.02.

respectively. The shape of the undoped PANI is octahedral shape and the diameter of the particles is 1 micrometer. In the case of doped PANI of different ratio shows different shapes. This is because the aniline monomer is likely to be adsorbed onto the surface of Co_3O_4 through electrostatic attraction and by the formation of weak charge-transfer complexes between aniline monomer and the structure of Co_3O_4. As a result of this adsorption process, Co_3O_4 are finely coated by PANI particles by the polymerization of aniline monomer. Thus, it is suitably believed that adsorption probability of aniline monomer on the whole surface of Co_3O_4 is equipotent, which results in the formation of continuous PANI coating on the surface of Co_3O_4. Therefore, the change in surface morphology causes the porosity of the PANI which increases with the Co_3O_4.

5 .3 FTIR spectrums of the undoped and Co_3O_4 doped PANI

Fourier transform infra-red (FTIR) spectra of undoped PANI and PANI / Co3O4 samples are recorded in the transmission range 400 to 4000 cm^{-1} are shown in Fig.8 . In a spectrum the band observed at 3452 cm^{-1} is due to N-H stretching. The polymer shows the broad .peak at 2375 cm^{-1} is associated with NH+ unsaturated amine. The absorption peaks observed around 1591 cm^{-1} is attributed to C=C stretching vibration of the quinoid ring. FTIR spectra of all the samples show strong absorption band in the region 750-1500 cm^{-1}, which correspond to the characteristics of PANI. The absorbance band at around 767 cm^{-1} observed show characteristics peaks of the C-H out-of plane bending vibration of the 1, 4-disubtituted benzene ring. The observed peak around 1112 cm^{-1} for undoped C-H bending vibration and observed peaks around 1357 cm^{-1} C-N stretching vibration. These results are in good agreement with the previous spectroscopic characterization of polyaniline. The observed peaks around at 2375 cm^{-1}, 3428 cm^{-1} for the undoped PANI and different ratio of PANI / Co_3O_4 nanocomposite can be probably related to the valence oscillation of the C-H and N-H bond stretching within the benzene rings, which have been associated with electrical conductivity and high degree of electron delocalization in PANI.

The splitting and intensity of absorption band on increasing the Co_3O_4 ratio suggest the presence of higher extent of protonation in these samples. For the PAni-Co_3O_4 composites, its IR-spectrum is almost identical to that of the pure PANI but all band shifts slightly towards the red side, and the intensity ratio of quinonoid band has also changed. These results indicate that some interactions exist between PANI and Co_3O_4 nanoparticles.

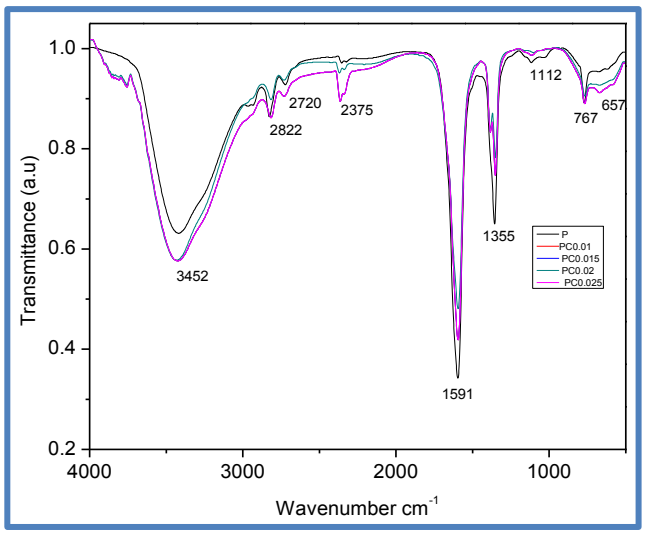

Figure 8. FTIR spectrum of samples P, PC0.01, PC0.015, PC0.02 and PC0.025

5.4 UV-visible Absorption Spectra of the undoped and Co_3O_4 doped PANI

The UV–visible absorption spectra of the undoped PANI and the PANI/ Co_3O_4 nanocomposite are recorded at room temperature by using a spectrophotometer between the wavelength range 200–800 nm as shown in Fig. 9. The sample P show single broad peak at around 446 nm. The

peak 446 nm is associated with the exciton transition of π-π*.

The longer wavelength peak at around 446 nm can be associated to the transition between benzene to quinoline rings. Intensity of the peak is randomly varied as the dopant concentration increased. There are two peaks at around 462 nm and visible region indicates high wavelength polar band or p-polar transition of emeraldine salt are observed in case of PC 0.01 and PC 0.02 ratio. The spectra reveal a characteristic two absorption peaks of composite material at 350 nm and 442 nm correspond to π-π* transition of C=N and polar on-π* transition of C-N+. The absorbance increases in the higher wavelength side indicating the role of Co_3O_4 nanoparticles.

It can be seen from the fig 8, that the λmax of pani has undergone a blue shift (hypsochromic) from 478nm and 469 nm as the concentration of Co_3O_4 increased from 0.01 to 0.02

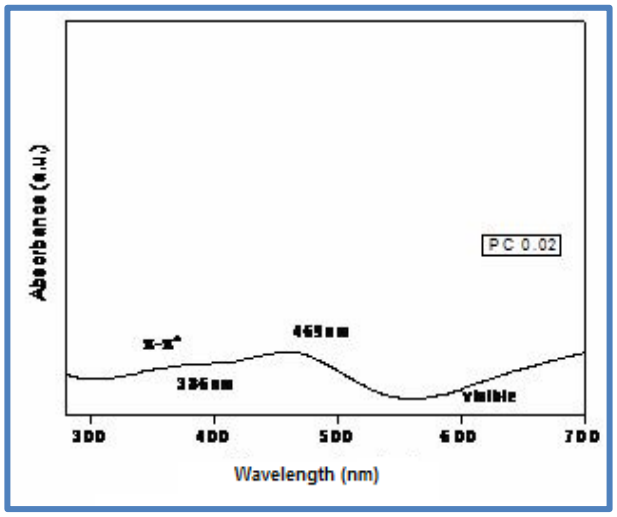

Figure 9 UV–visible absorption spectra for the samples P, PC0.01 and PC 0.02.

5.5 Photoluminescence Studies of the undoped and Co_3O_4 doped PANI

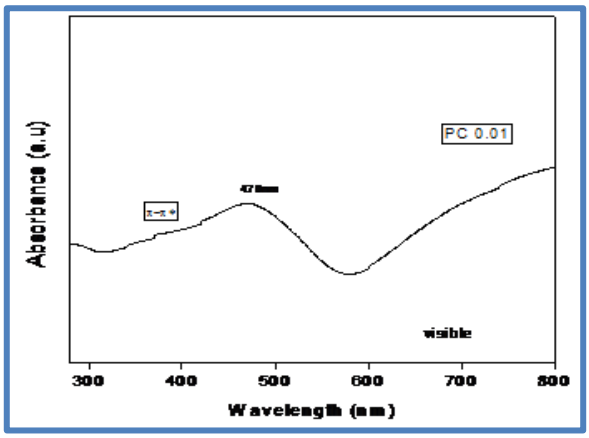

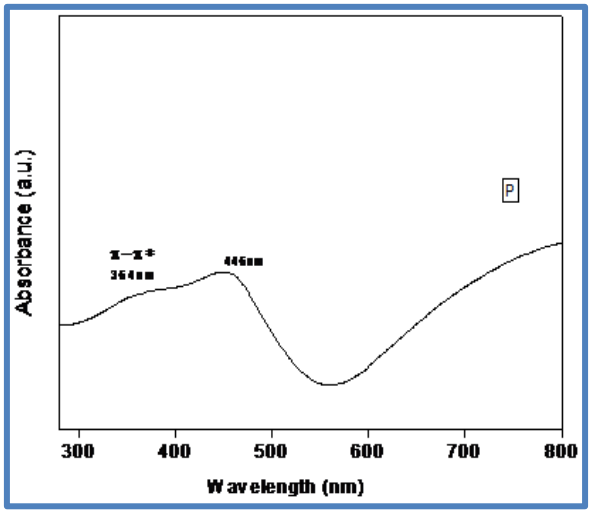

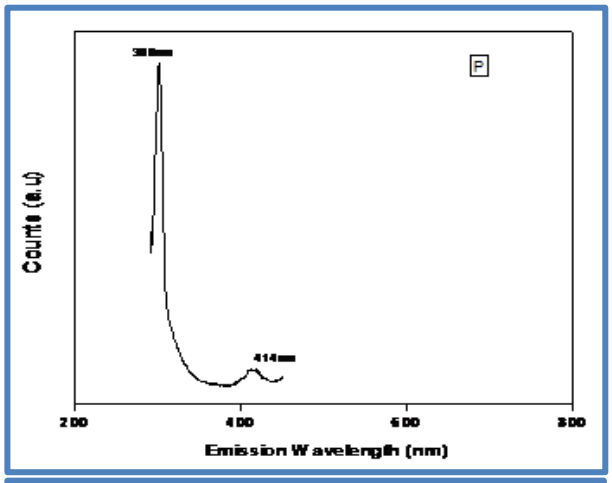

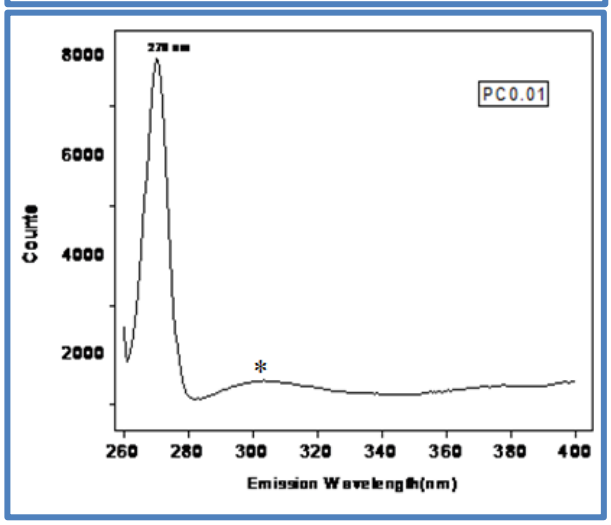

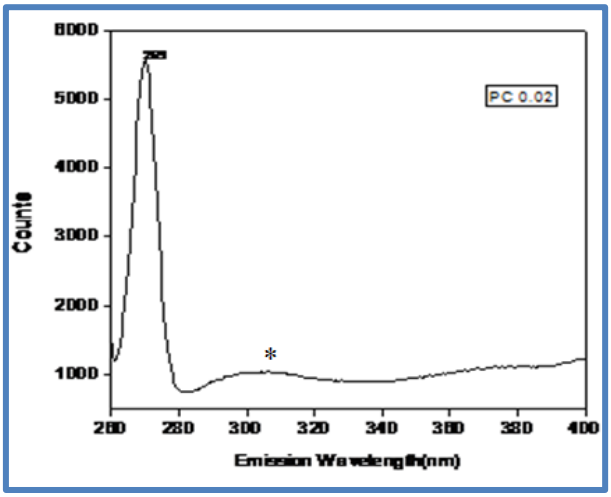

Figure 10 Photoluminescence (PL) spectra for the samples P, PC0.01 and PC 0.02.

5.6 Zeta Potential Measurements of the undoped and Co_3O_4 doped PANI

Zeta potential is a parameter characterizing electrochemical equilibrium on interfaces. It depends on the properties of liquid as well as on properties of the surface. It plays an important role in theory of aggregative stability – DLVO theory. Electrostatic repulsion between particles depends on the value of zeta potential. The higher the zeta potential, the stronger the repulsion, the more stable the system becomes. For instance, high zeta potential of the fat droplets in milk prevents them against coalescence. Reduction of it due to addition of acid would lead to cheese formation from coalescence droplets.

Table 3 Zeta-Potential Values of used materials

Sample	Zeta potential (mV)	Conductivity (S/cm)
C	-0.292	0.0423
P	-4.79	0.0467
PC0.01	41.8	0.539
PC0.02	27.5	0.199

Measurements of zeta potential were also carried out in order to study the stability of nanoparticles as this extremely important for many applications, Surface zeta potentials were measured using the zeta analyzer (Malvern ZS – Zeta size) Liquid samples of the nanoparticles (5ml) were diluted with double distilled water (50 mL) and the pH was then adjusted to the required value. The samples were shaken for 30 minutes. After shaking the zeta potential of the metallic particles was measured.

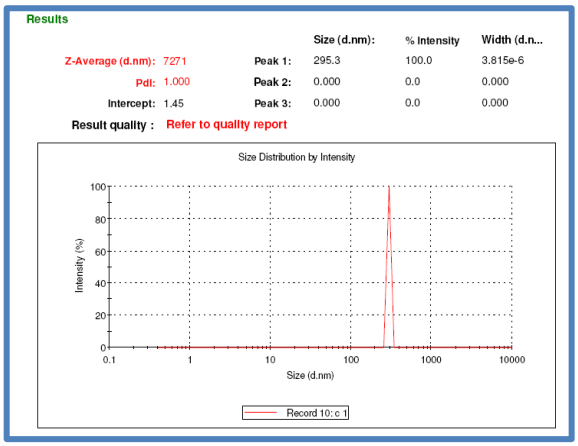

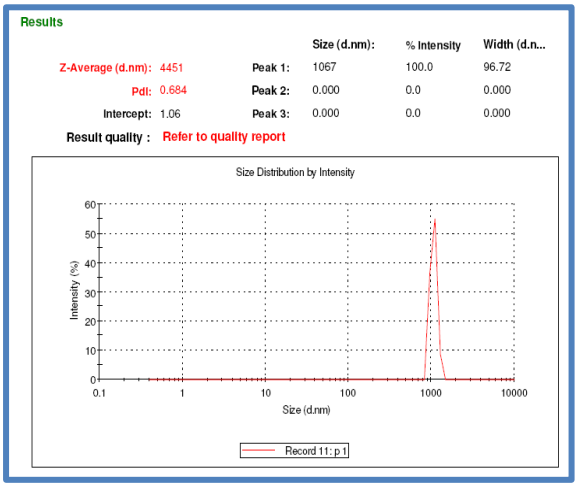

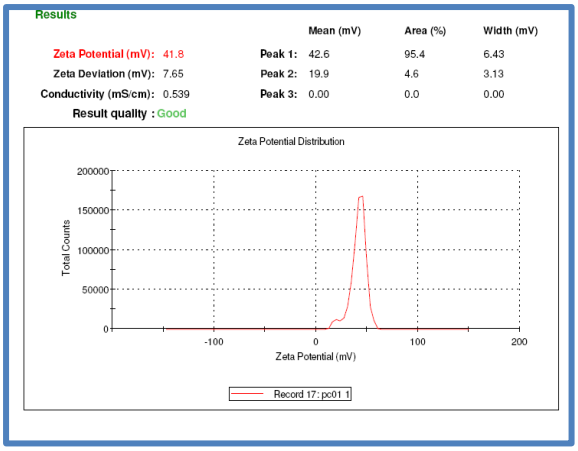

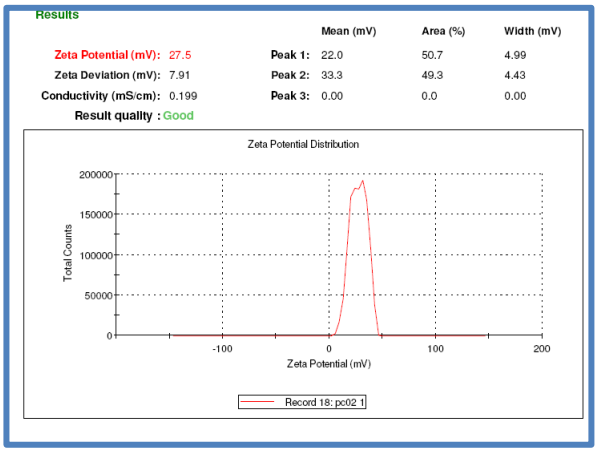

Figure 11 Zeta potential for the samples P, PC0.01 and PC0.02.

The possible electrostatic charge on the surface of the Co_3O_4 NPs synthesized has been investigated by zeta potential analysis. The zeta potential has been studied at the same pH of the corresponding NPs–PANI mixture. The obtained results of zeta potential distribution have been shown in Fig. 11.

Both Co NPs (-0.292) and PANI (-4.79) show negative zeta potentials like. This behavior unambiguously suggests the presence of strong electric charges on the particle surfaces to hinder agglomeration. These values were found to fall in the negative side which showed the efficiency of the capping materials in stabilizing the nanoparticles by providing intensive negative charges that keep all the particles away from each other. In case of PC0.01 and PC0.02 show quite high zeta potential than Co3O4 NPs. Thus, the nucleation of the electroactive phase takes place on the negatively charged surfaces of Co NPs. The positive NH2 dipoles of PANI chains undergo strong electrostatic interaction with the negatively charged surface of the NPs

5.7 Dielectric constant of the undoped and Co_3O_4 doped PANI

The dielectric constant is the ratio of the permittivity of a substance to the permittivity of free space. It is an expression of the extent to which a material concentrates electric flux, and is the electrical equivalent of relative magnetic permeability. As the dielectric constant increases, the electric flux density increases, if all other factors remain unchanged. This enables objects of a given size, such as sets of metal plates, to hold their electric charge for long periods of time, and/or to hold large quantities of charge. Materials with high dielectric constants are useful in the manufacture of high-value capacitors.

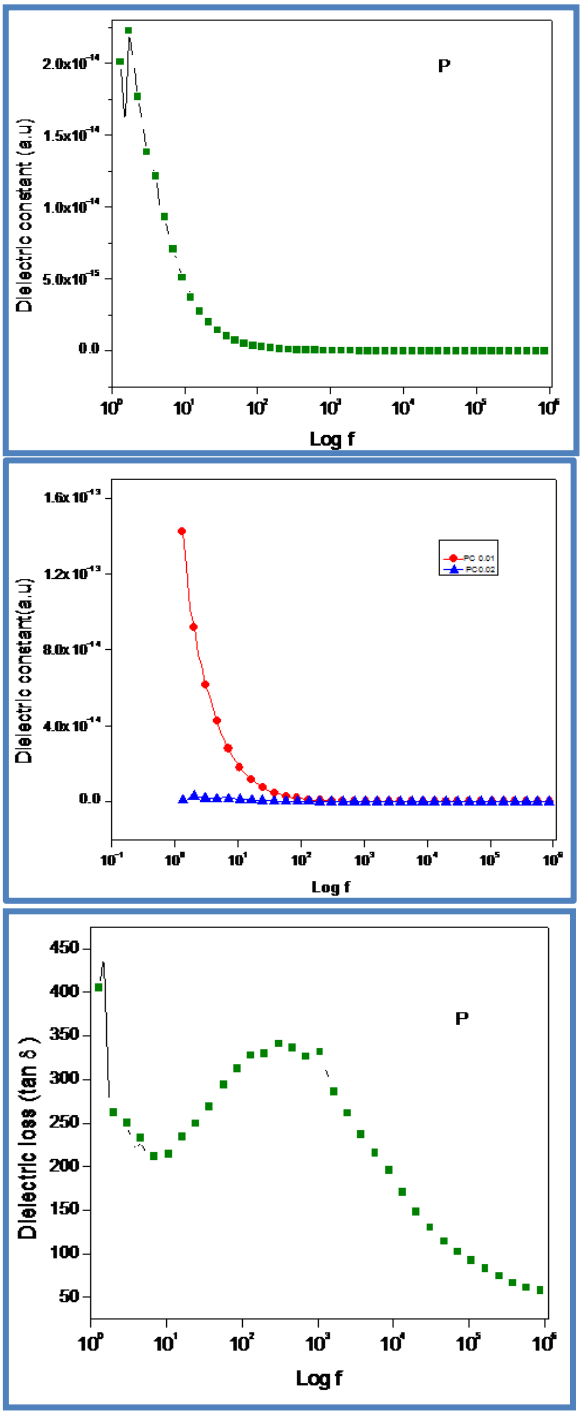

Fig. 12 (a) Dielectric constant **(b)** Dielectric loss for the samples P, PC0.01 and PC 0.02.

A high dielectric constant, in and of itself, is not necessarily desirable. Generally, substances with high dielectric constants break down more easily when subjected to intense electric fields, than do materials with low dielectric constants. For example, dry air has a low dielectric constant, but it makes an excellent dielectric material for capacitors used in high-power radio-frequency (RF) transmitters. Even if air does undergo dielectric breakdown (a condition in which the dielectric suddenly begins to conduct current), the breakdown is not permanent. When the excessive electric field is removed, air returns to its normal dielectric state. Solid dielectric substances such as polyethylene or glass, however, can sustain permanent damage.

Fig.12a shows variation of dielectric constant as a function of frequency for pure polyaniline and Co_3O_4 composite (PC0.01 and PC0.02). It is observed that at low frequencies dielectric constant was found to decrease with increasing frequency. And then above 1 MHz dielectric constant is found to increase with increase in frequency, which is the characteristic feature of disordered materials. This could be due to the fact that ions are unable to oppose the effects of the field and/or tightly pinned to the polymer chain.

Fig. 12 b. show variation of dielectric loss as a function of frequency for pure polyaniline and Co_3O_4 composite (PC0.01 and PC0.02). It is observed that the dielectric loss tangent in case of polyaniline and its composite increases as a function of frequency. Both polyaniline and its composites exhibit small value of dielectric loss at higher frequency. And it is observed that the dielectric loss increases in ratio of PC 0.02 compared to PC0.01, These values go in accordance with the values of dielectric constant.

5.8 Photocatalytic Activity

Accumulation of a substance between the liquid–solid interface or gas–solid interface due to physical or chemical associations is termed an adsorption process. With few exceptions, adsorption is usually controlled by physical parameters on most of the adsorbents such as polarity, van der Waals forces, hydrogen bonding, dipole–dipole interaction, π–π interaction, etc. Therefore, the design of an adsorbent usually depends on the type of substance to be adsorbed or removed.

A Stock solution of MO was prepared with distilled water. Dilution was made depending on the desired dye concentration. Proper amount of catalyst was added to the dye solution at the beginning of the experiment.

As the decolourization of Methyl orange precedes time dependent UV-Vis spectra was recorded. Fig .13 shows the UV-Vis spectra of MO dye as a function of time in presence of sample. It was observed that the absorbance value of MO decreases with increases in the time of irradiation.

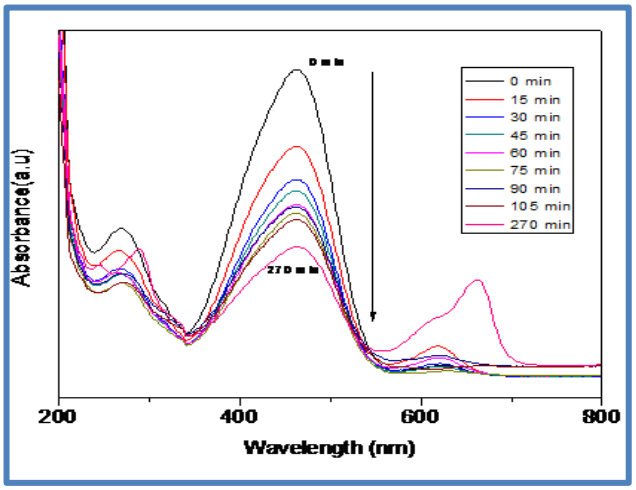

Figure 13 Photocatalytic Activity of PC0.01 with Methyl Orange.

6 Conclusions

In this paper, the conducting polymer/metal oxide composites have been synthesized using in-situ chemical oxidative polymerization method of using potassium persulfate as oxidant. The polymer/metal oxide composites were characterized by X-ray diffraction, Fourier transform infrared, Scanning electron microscopy, UV absorption, Photoluminescence. Fourier transform infrared (FTIR) spectroscopy, confirms the presence of metal oxide in the polymer structure. The SEM micrograph clearly reveals the dispersion of Co_3O_4 nanoparticles in PANI Matrix. In other words, metal oxide particles are embedded in polymer matrix. In XRD spectrum shows the average particle size of P is 2.6nm. The average particle size of PC0.01 and PC0.02 is 3.3 nm and 7.03 nm respectively. This result shows that the metal oxide concentration increases the average particle size also increases. A Photoluminescence spectrum shows some electronic changes occur in polymer /metal oxide

nanocomposite. The Zeta potential value PC0.01 and PC0.02 shows high zeta potential than Co_3O_4 NPs. Thus, the nucleation of the electroactive phase takes place on the negatively charged surfaces of Co NPs. The dielectric loss increases in ratio of PC 0.02 compared to PC0.01, These values go in accordance with the values of dielectric constant.

References

[1] K. H. Liao, A. Mittal, S. Bose, C. Leighton, K. A. Mkhoyan, C. W. Macosko, Aqueous Only Route toward Graphene from Graphite Oxide, *ACS Nano*, 5 (2011) 1253-1258.

[2] X. G. Mei, J. Y. Ouyang, Ultrasonication-assisted ultrafast reduction of graphene oxide by zinc powder at room temperature, *Carbon*, 49 (2011) 5389-5397.

[3] R. S. Dey, S. Hajra, R. K. Sahu, C. R. Raj, M. K. Panigrahi, A rapid room temperature chemical route for the synthesis of graphene: metal-mediated reduction of graphene oxide, *Chemical Communications*, 48 (2012) 1787

[4] Y. M. Shul'ga, V. N. Vasilets, S. A. Baskakov, V. E. Muradyan, E. A. Skryleva, Y. N. Parkhomenko, Photoreduction of graphite oxide nanosheets with vacuum ultraviolet radiation, *High Energy Chemistry*, 46 (2012) 117-121.

[5] A. Wei, J. Wang, Q. Long, X. Liu, X. Li, X. Dong, W. Huang, Synthesis of high-performance graphene nanosheets by thermal reduction of graphene oxide, *Materials Research Bulletin*, 46 (2011) 2131-2134.

[6] J. T. Paci, T. Belytschko, G. C. Schatz, Computational Studies of the Structure, Behavior upon Heating, and Mechanical Properties of Graphite Oxide, *Journal of Physical Chemistry C*, 111 (2007) 18099-18111.

[7] K. Zhang, L. L. Zhang, X.S. Zhao, J. Wu, Graphene/Polyaniline Nanofiber Composites as Supercapacitor Electrodes, *Chemistry of Materials*, 22 (2010) 1392-1401.

[8] H. Wang, Q. Hao, X. Yang, L. Lu, X. Wang, Graphene oxide doped polyaniline for supercapacitors, *Electrochemistry Communications*, 11 (2009) 1158-1161.

[9] F. Li, J. Song, H. Yang, Q. Zhang, S. Gan, D. Han, A. Ivaska, L. Niu, One-step synthesis of graphene/SnO_2 nanocomposites and its application in electrochemical supercapacitors, *Nanotechnology*, 20 (2009) 455602

[10] J. Yan, Z. Fan, T. Wei, W. Qian, M. Zhang, F. Wei, Fast and reversible surface redox reaction of graphene–MnO2 composites as supercapacitor electrodes, *Carbon*, 48 (2010) 3825-3833.

[11] C. C. Hu, K. H. Chang, M. C. Lin, Y. T. Wu, Design and Tailoring of the Nanotubular Arrayed Architecture of Hydrous RuO_2 for Next Generation Supercapacitors, *Nano Letters*, 6 (2006) 2690-2965.

[12] L. Z. Fan, Y. S. Hu, B. Smarsly, J. Maier, P. Adelhelm, M. Antonietti, High Electroactivity of Polyaniline in Supercapacitors by Using a Hierarchically Porous Carbon Monolith as a Support, *Advanced Functional Materials*, 17 (2007) 3083–3087.

[13] Z. A. Hu, Y. L. Xie, Y. X. Wang, L. J. Xie, G. R. Fu, X. Q. Jin, Z. Y. Zhang, Y. Y. Yang, H. Y. Wu, Synthesis of α-Cobalt Hydroxides with Different Intercalated Anions and Effects of Intercalated Anions on Their Morphology, Basal Plane Spacing, and Capacitive Property, *Journal of Physical Chemistry C*, 113 (2009) 12502–12508.

[14] S. Stankovich, R. D. Pine, K. A. Kohlhaas, A. Kleinhammes, Y. Jia, Y. Wu, S. T. Nguyen, D. A. Dikin R. S. Ruoff, Synthesis of graphene-based nanosheets via chemical reduction of exfoliated graphite oxide, *Carbon*, 45 (2007) 1558-1565.

[15] N. I. Kovtyukhova, P. J. Ollivier, B. R. Martin, T. E. Mallouk, S. A. Chizhik, E. V. Buzaneva, A. D.Gorchinskiy, Layer-by-Layer Assembly of Ultrathin Composite Films from Micron-Sized Graphite Oxide Sheets and Polycations, *Chemistry of Materials*, 11 (1999) 771-778.

Acknowledgement

This research received no specific grant from any funding agency in the public, commercial, or not-for-profit sectors.

Competing Interests:

The authors declare that they have no competing interests.

About The License